Structural and gas-sensing properties of CuO-CuxFe3–xO4 nanostructured thin films

Audrey Chapelle, Mohd H. Yaacob, Isabelle Pasquet, Lionel Presmanes, Antoine Barnabé, Philippe Tailhades, Johan Du Plessis, Kourosh Kalantar-Zadeh

HAL Id: hal-00717490

https://hal.science/hal-00717490

Submitted on 13 Jul 2012

Structural and gas-sensing properties of CuO–Cu$_x$Fe$_{3-x}$O$_4$ nanostructured thin films

Audrey Chapelle [a,*], Mohd H. Yaacob [c,d], Isabelle Pasquet [a], Lionel Presmanes [a], Antoine Barnabé [a], Philippe Tailhades [a], Johan Du Plessis [b], Kourosh Kalantar-zadeh [c]

[a] Institut Carnot CIRIMAT, Université Paul Sabatier, Toulouse, France
[b] Applied Physics, School of Applied Sciences, RMIT University, Melbourne, Australia
[c] School of Electrical and Computer Engineering, RMIT University, Melbourne, Australia
[d] Faculty of Engineering, Universiti Putra Malaysia, Serdang, Selangor, Malaysia

ABSTRACT

Nanocrystalline CuO–Cu$_x$Fe$_{3-x}$O$_4$ thin films were developed using a radio-frequency sputtering method followed by a thermal oxidation process. Thin films were deposited applying two very different conditions by varying the argon pressure and the target-to-substrate distance. Structural, microstructural and gas-sensing characteristics were performed using grazing incidence X-ray diffraction (GXRD), Raman spectroscopy, atomic force microscopy (AFM), X-ray photoelectron spectroscopy (XPS), transmission electron microscopy (TEM), scanning electron microscopy (SEM), and electrical measurements. Their sensing properties were examined using hydrogen gas in dry synthetic air. The shortest response and recovery times were observed between 280 and 300 °C independently of the deposition conditions.

1. Introduction

Hydrogen is a colorless and odorless gas, and such, its leakage cannot be noticed easily. As hydrogen is highly flammable, any potential leak can present an explosion hazard. Thus, there is a great demand and subsequent challenges for monitoring hydrogen levels for the purpose of control and safety applications in domestic and industrial fields [1]. Metal oxide semiconductors, such as CuO and its composites, have been the subject of interest for a many years for the detection of reducing gases such as H$_2$ [2–4], C$_2$H$_5$OH [5], CO [6–9], and H$_2$S [10,11]. The gas sensing properties of these metal oxide semiconductors are influenced by many factors such as their operating temperatures, morphology and chemical composition. CuO is especially an interesting metal oxide for gas sensing. It is an intrinsically p-type semiconductor with a bandgap in the range of 1.2–1.4 eV [12–14] and its properties can be altered upon mixing with other metals and metal oxides. The interest for nanocomposites and p–n heterojunctions is growing in the field of gas sensing. Some authors have reported that by the association of a metal oxide with CuO, and forming mixtures such as CuO/ZnO, CuO/SnO$_2$, high sensitivity and selectivity to reducing gas species can be exhibited [15–18]. Among such metal oxide mixtures, spinels present interesting semiconducting properties due to the mixed valence of the elements. Spinels in general are known for their catalytic properties which enable changes in the electronic behaviors. There are several reports on spinel oxide composites capabilities for gas sensing [19–21]. In this work, Cu$_x$Fe$_{3-x}$O$_4$ has been chosen for its n-type semiconducting property, as well as the possibility of forming into nanocomposites thin films with CuO [22,23]. By changing the Cu and Fe contents, the material can be tuned in a wide range of conductivities and altered from n- to p-type. Subsequently, the band-gap can also be tuned within a broad range.

Radio-frequency (RF) sputtering is a reliable and well controlled method in the preparation of nanocomposite thin films with a good homogeneity and crystallinity at low substrate temperature [24,25]. It has been shown that the physical and chemical properties of the growing layer depend on the deposition conditions such as pressure, magnetron, target-to-substrate distance and substrate temperature [22,26]. Consequently, changing the sputtering conditions alters the microstructure and the stoichiometry of the deposited thin films [27,28].

In the present paper, we report the structural and gas-sensing properties of CuO-Cu$_x$Fe$_{3-x}$O$_4$ nanocomposite thin films obtained

Target	CuFeO$_2$	
Magnetron	No	
RF power (W)	200	
Argon pressures (Pa) P	0.5	2
Target-to-substrate distance (cm) d	5	8
Deposition rates (nm/min)	6.8	3.5
Substrate	Glass	

by RF-sputtering. Mixing of different metal oxides and the formation of binary compounds can make the resulting mixture selective to target gas species [29,30]. As a result, there have been a large number of reports on the formation of such binary metal oxide and reports as how the change of concentration of one metal oxide with reference to other can be used for tuning the gas sensing properties [31–33]. The structures and morphologies of the films were studied by grazing incidence X-ray diffraction (GXRD), Raman spectroscopy, atomic force microscopy (AFM), scanning electron microscopy (SEM) and X-ray photoelectron spectroscopy (XPS). Device's resistance was investigated as a function of operating temperatures and different H$_2$ gas concentrations.

2. Experimental

2.1. Synthesis of CuO–Cu$_x$Fe$_{3-x}$O$_4$ nanocomposites

Cu–Cu$_x$Fe$_{3-x}$O$_4$ thin films were deposited with Alcatel A450 apparatus using a custom-made sintered ceramic target of pure CuFeO$_2$ with a relative density of 70%. The RF power was set at 200 W and the pressure inside the deposition chamber was lower than 5×10^{-4} Pa prior to the deposition. All studied films were deposited on pre-cleaned substrates which were placed on a water cooled sample holder. No additional heating was required during the deposition. The target was pre-sputtered in an argon plasma for 10 min to remove surface contamination prior to the process. The depositions were carried out with various argon pressures (P) and target-to-substrate distances (d) ranging from 0.5 Pa to 2 Pa and 5 cm to 8 cm, respectively. The deposition conditions are summarized in Table 1. Films with the thicknesses in the range of 100 nm to 600 nm were deposited onto substrates for structural characterizations. The deposition rates of thin films at different conditions are presented in Table 1.

The CuO–Cu$_x$Fe$_{3-x}$O$_4$ nanostructured films were obtained by the thermal treatment of the as-deposited layers in air at 450 °C for 12 h. Comb-type interdigitated electrodes were patterned on the top of the annealed thin films via the sputter deposition of 50 nm thick gold through a metal shadow mask (as shown in Fig. 1). Afterwards, two gold wires were bonded to the gold electrode using silver epoxy.

2.2. Characterization and gas sensing property measurements

The GXRD patterns (grazing angle $\alpha = 1°$) were obtained with a Siemens D5000 diffractometer using the Cu Kα radiation. The surface morphology of the thin films were determined by a Veeco Dimension 3000 AFM equipped with a super sharp TESP-SS Nanoworld© tip (nominal resonance frequency 320 kHz, nominal radius curvature 2 nm) and JEOL 2100 TEM operating at 200 kV equipped with a X-ray energy dispersive spectroscopy (X-EDS) system. The SEM images were obtained using a field emission gun Jeol JSM 6400. The Raman spectra were collected under ambient conditions using a modular Olympus BX41 Raman microscope (Horiba Jobin Yvon) fitted with a 50× objective lens, through which spectra were excited using a fiber-coupled 532 nm laser and power of 1.1 mW. The scattered signal was gathered by the same 50× objec-
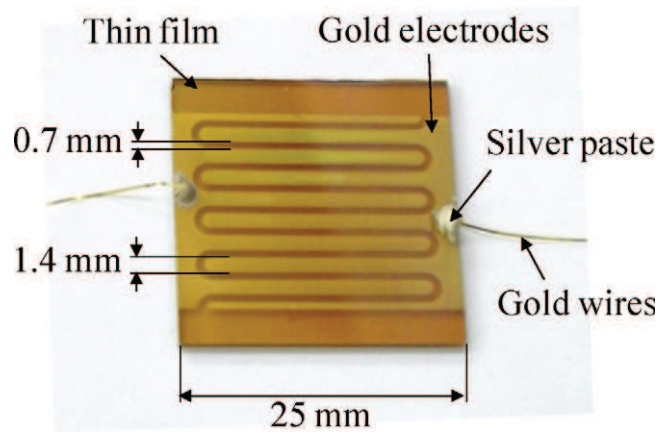

Fig. 1. Picture of the device used for electrical testing of the CuO–Cu$_x$Fe$_{3-x}$O$_4$ thin films.

tive lens in a backscattering configuration and was then coupled to a spectrometer (Jobin Yvon Triax 320), which was fitted with a thermoelectrically cooled CCD detector. In all cases, 5 accumulations of 30 s each were averaged together. A Thermo Scientific K-Alpha apparatus was used for XPS measurements using a monochromatic Cu Kα radiation with a 400 μm spot size. Survey and peaks were scanned at 200 and 50 eV pass energy, respectively. Flood gun was used to minimize charging effects.

For the gas sensing measurements, the CuO–Cu$_x$Fe$_{3-x}$O$_4$ based sensors were mounted on a heater in a Teflon chamber. The heater was controlled by a regulated DC power supply providing different operating temperatures. The sensor output resistance as a function of time was recorded using a multimeter (Keithley 2001), while the gases were continuously flown through the chamber at a total flow rate of 200 sccm. A computerized gas calibration system, with
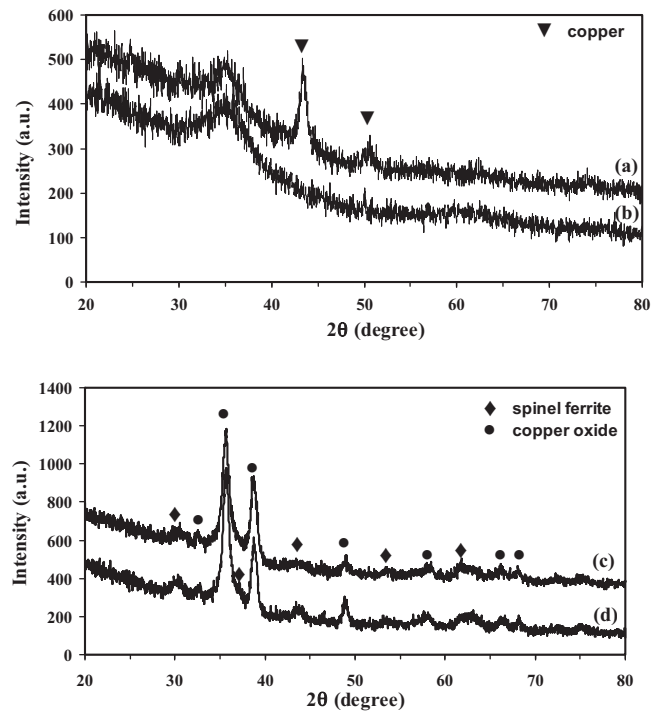

Fig. 2. Grazing angle X-ray diffraction patterns of as-deposited samples at different deposition conditions, (a) P$_{0.5}$d$_5$, (b) P$_2$d$_8$ and annealed samples in air at 450 °C (c) P$_{0.5}$d$_5$, (d) P$_2$d$_8$.

mass flow controllers, was used for exposing the sensor to the desired concentrations of H_2 gas coupled with dry synthetic air used as the reference gas. The sensor response S was defined as $S (\%) = ((R - R_0)/R_0) \times 100$, where R_0 is the resistance of the sensor in dry air, and R is the resistance of the sensor under hydrogen flow.

3. Results and discussion

3.1. Structural analysis

Sample $P_{0.5}d_5$ was deposited at low pressure (0.5 Pa) and low target-to-substrate distance (5 cm), while sample P_2d_8 was pre-
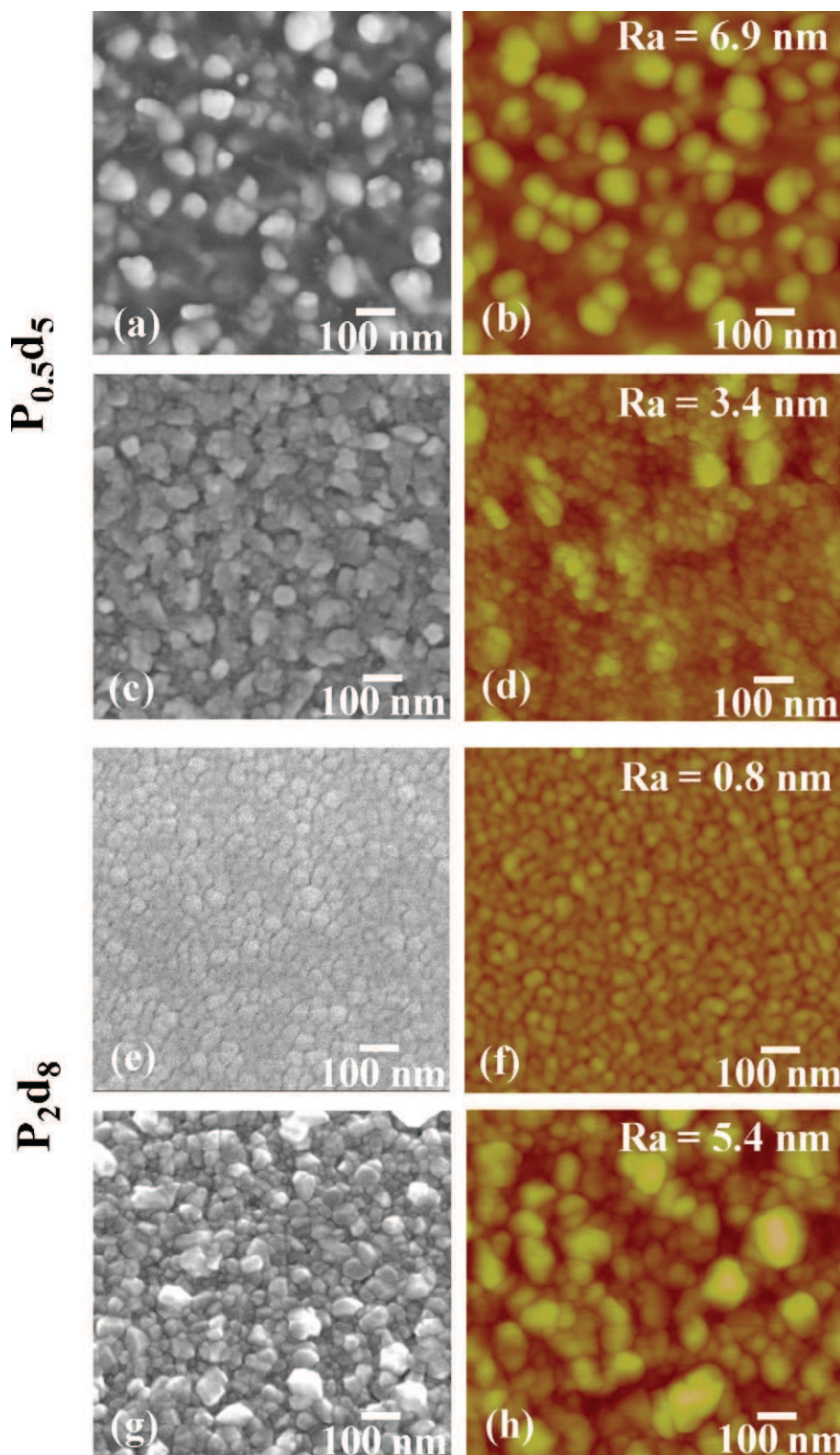

Fig. 3. SEM and AFM images of samples obtained at different deposition conditions, (a and b) $P_{0.5}d_5$ as-deposited, (c and d) $P_{0.5}d_5$ annealed in air at 450 °C, (e and f) P_2d_8 as-deposited, (g and h) P_2d_8 annealed in air at 450 °C. Ra represents the roughness.
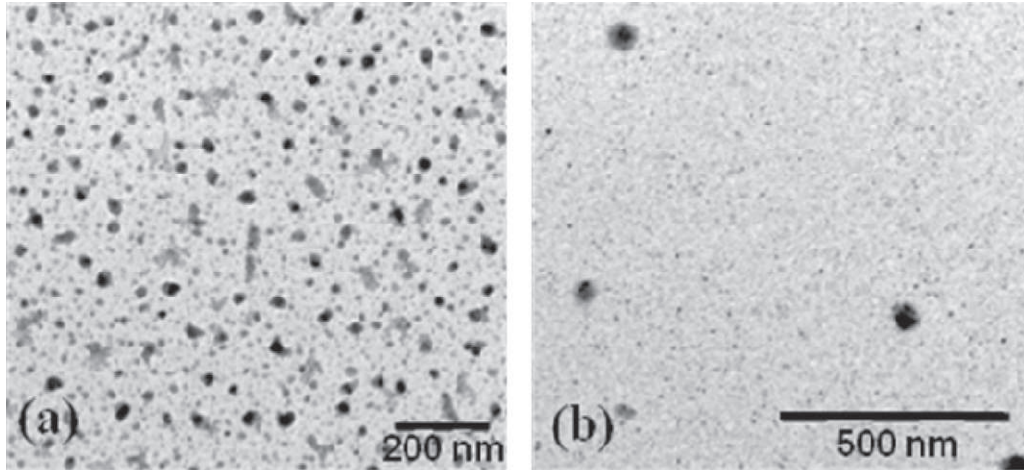
Fig. 4. TEM images of as-deposited samples at (a) $P_{0.5}d_5$ and (b) P_2d_8.

pared at higher pressure (2 Pa) and higher target-to-substrate distance (8 cm). The deposition conditions were adjusted [22] in order to obtain either much reduced phases than that of the target ($CuFeO_2$) or phases with the same oxygen content.

Fig. 2 shows the GXRD patterns of the as-deposited samples using the two different deposition conditions. A broad peak is observed at $2\theta = 35.5°$, i.e $d_{hkl} \approx 2.5$ Å, which could be attributed to various mixed oxide phases such as Cu_2O ($d_{111} = 2.46$ Å), CuO ($d_{11-1} = 2.52$ Å), $CuFeO_2$ ($d_{012} = 2.51$ Å), $Cu_xFe_{3-x}O_4$ ($0 < x < 1$) ($d_{311} = 2.50$ Å–2.52 Å) as reported previously [34]. At low pressures, the mean free path of the particles ejected from the target is higher and they are more energetic, as these particles face a smaller number of collisions during the transfer from the target to the substrate. As a result for sample $P_{0.5}d_5$, the particles arriving on the growing layer are more energetic and tend to re-bombard the growing layer (especially the oxygen atoms in the layer, which are light elements). The consequence of the re-bombardment is a layer, which is more reduced than the target. In this case, the equilibrium diagram of the Cu–Fe–O system [35] predicts a mixture of copper (Cu) and spinel ferrite ($Cu_xFe_{3-x}O_4$). However, the sputtering technique provides an out-of-equilibrium reaction and thus the reduction is only partial. Consequently, we obtain a thin film composed of both metallic copper and an oxide mixture of spinel ferrite and delafossite phase ($CuFeO_2$). Copper tends to crystallize much easier than the two other oxides, which explain the GXRD pattern (Fig. 2a). The two other oxides are nanocrystalline, which give the GXRD pattern a broad peak. Inversely for the P_2d_8 deposition, as the mean free paths of particles leaving the target are lower, they are less energetic. Therefore, the stoichiometry of the growing layer is close to the target and no metallic copper is detected by the GXRD (Fig. 2b).

The GXRD patterns of the annealed samples in air for 12 h at 450 °C are shown in Fig. 2c and d. This treatment leads to the formation of two phases predicted by the Cu–Fe–O system [35], which are associated well to copper oxide and spinel ferrite.

The SEM and AFM were performed on as-deposited samples and annealed samples in air at 450 °C for 12 h. Fig. 3 shows the morphologies obtained at different conditions for the 300 nm thick sample. For $P_{0.5}d_5$ (Fig. 3a and b), the average particle diameter is approximately 60 nm with a relatively high roughness of almost 7 nm, which is due to the presence of metallic crystallized copper particles, tending to increase the roughness. On the other hand, for P_2d_8 (Fig. 3e and f) the thin film shows a smoother surface (Ra = 1 nm) with the average particle diameter of approximately 35 nm. In confirmation, the metallic copper was also not detected by the GXRD pattern (Fig. 2b), which explains why the surface roughness is smaller.

The thermal treatments in air of the as deposited layers lead to the formation of increasingly crystalline CuO–$Cu_xFe_{3-x}O_4$ composite as confirmed by the GXRD patterns (Fig. 2c and d), where the copper oxide originates from either the oxidation of the metallic copper or the decomposition of the $CuFeO_2$ phase. However, their microstructures remain different. Fig. 3c and d shows an agglomeration of small grains involving increasingly compact structure for $P_{0.5}d_5$ and Fig. 3g and h exhibits larger grains within P_2d_8 with a higher roughness and seems to be more porous than $P_{0.5}d_5$. It has been demonstrated [36] that films prepared with a sputtering argon pressure of 0.5 Pa and a target-to-substrate distance of 5 cm are usually very dense. It has also been reported that increasing the pressure and/or target-to-substrate distance augment the porosity of the films [36]. As it is generally assumed, the porosity results from shadowing effects lead to a small mean free path λ for the atoms in the plasma. At high pressure deposition, the atoms reach the substrate in an oblique incidence, forming crystallites that produce localized shadow zones, which hinders the homogenous deposition of the films, hence enhances the porosity. The angle of incidence also becomes higher by increasing the target-to-substrate distance, which affects the deposited film similarly.

The TEM was performed for the as-deposited samples with a thickness of 30 nm on carbon covered nickel grid ($P_{0.5}d_5$ – Fig. 4a). The black dots were associated to metallic copper by X-EDS, which were also confirmed by the GXRD patterns. It can be seen that the sample obtained at low pressure–low distance is a nanocomposite of many metallic copper particles in an oxide matrix. The TEM image of the film obtained at high pressure-high distance (P_2d_8 – Fig. 4b) is mostly made of an oxide matrix. However, some large metallic particles were also observed even though no metallic copper was detected by the GXRD.

The Raman spectra of the as-deposited and annealed samples at different deposition conditions are presented in Fig. 5. All spectra were taken with a collection time of 2 min 30 s. The results in Fig. 5a and c show that the as-deposited thin films for both conditions are characterized by a broad band at 630 cm^{-1}. Copper is not expected to appear in these spectra since it is Raman silent as Cong et al. demonstrated [37]. The Raman spectra of annealed thin films at 450 °C are shown in Fig. 5b and d. Three bands were observed at 293, 340, and 623 cm^{-1} and a broad, but relatively strong feature appeared at 1100 cm^{-1}, which were all assigned to CuO [37–39]. The peak at 293 cm^{-1} seems to be more intense for P_2d_8 than $P_{0.5}d_5$, which means that this sample contains more copper oxide. It seems that the copper content in the sample with larger particle morphologies ($P_{0.5}d_5$) not completely turned into CuO after annealing, while the 450 °C annealing temperature appears
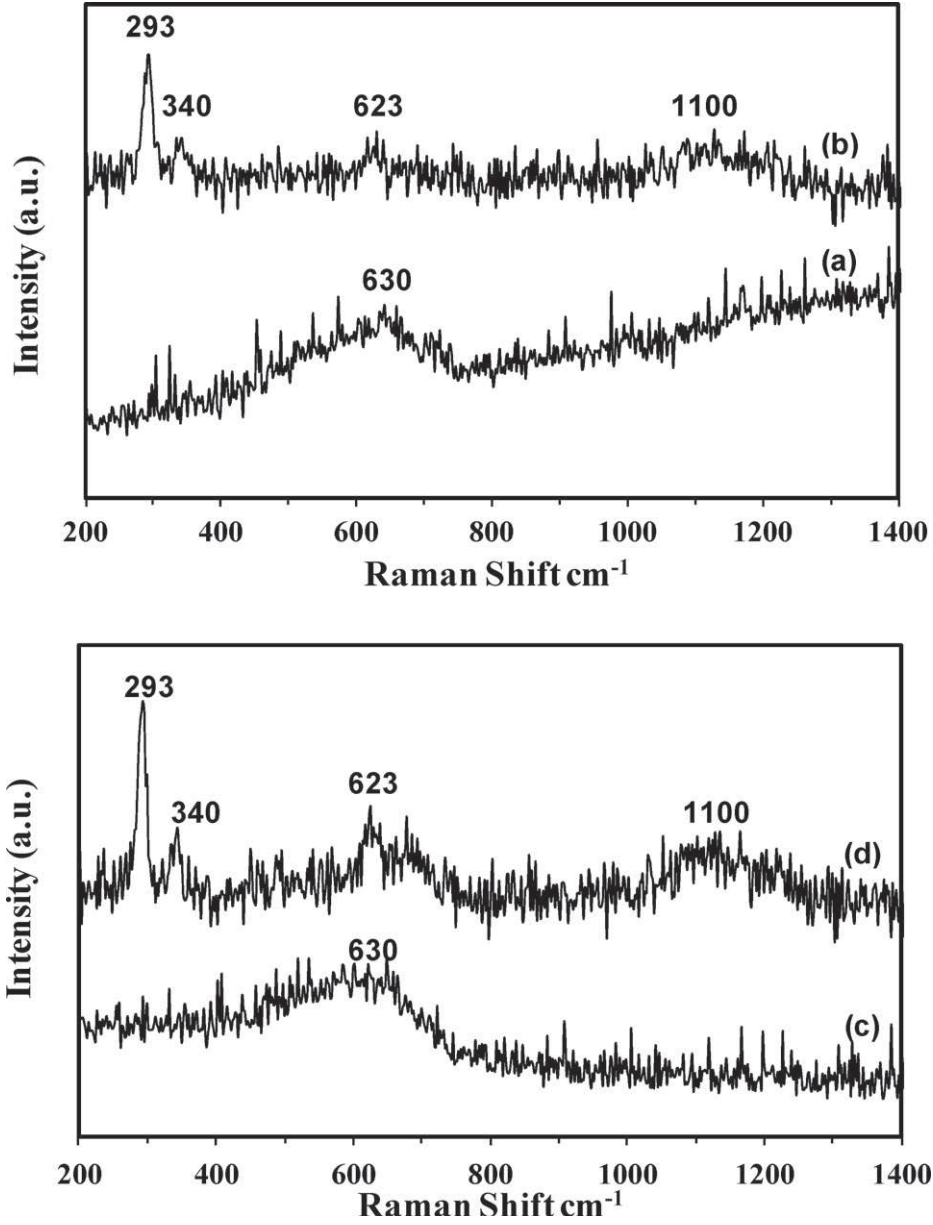
Fig. 5. Raman spectra of thin films: (a) $P_{0.5}d_5$ as-deposited, (b) $P_{0.5}d_5$ annealed at 450 °C in air, (c) P_2d_8 as-deposited and (d) P_2d_8 annealed at 450 °C in air.

to be more effective in transforming small particles of P_2d_8 into CuO.

3.2. Gas sensing results

The sensor responses to 0.125, 0.25 and 0.5% of H_2 (in dry air) at a temperature ranging from 220 to 310 °C are displayed in Fig. 6a and b. In our case, gas sensing experiments were performed in dry air atmosphere to avoid any interference from humidity. The maximum response of the sensor occurs at the temperature of 280 and 295 °C for sensors with $P_{0.5}d_5$ and P_2d_8 layers (thickness 100 nm), respectively. As can be seen in Fig. 7, the sensors showed good repeatability as the initial baseline was regained upon exposure to dry air.

The increase in the electrical resistance of the sensors upon exposure to a reducing gas such as H_2 indicates the presence of that the obtained films had p-type semiconducting properties. This implies the domination of CuO over $Cu_xFe_{3-x}O_4$, which is an n-type material.

Hoa et al. [40] suggested that behaviour of CuO based sensor originates from the interaction between the chemisorbed H_2 and the adsorbed oxygen on the sensor surfaces. They showed that when CuO is exposed to hydrogen, the H_2 molecules interact with CuO through the oxygen ions preadsorbed onto the CuO surface as described by Eqs. (1) and (2):

$$H_{2(ads)} + O^-{}_{(ads)} \leftrightarrow H_2O + e^- \tag{1}$$

$$H_{2(ads)} + O^{2-}{}_{(ads)} \leftrightarrow H_2O + 2e^- \tag{2}$$

At 0.125% H_2, the characteristic response and recovery times of the sensor at the operating temperature of 280 °C for $P_{0.5}d_5$ were 150 and 320 s, respectively, with a response S of 37% and at 295 °C for P_2d_8 were 190 and 400 s, respectively, with a response (S) of 40%. The difference in gas response between $P_{0.5}d_5$ and P_2d_8 can be ascribed to the morphologies of microstructures and difference in porosity, as describe in the previous section, as well as the nature of the phases in presence.
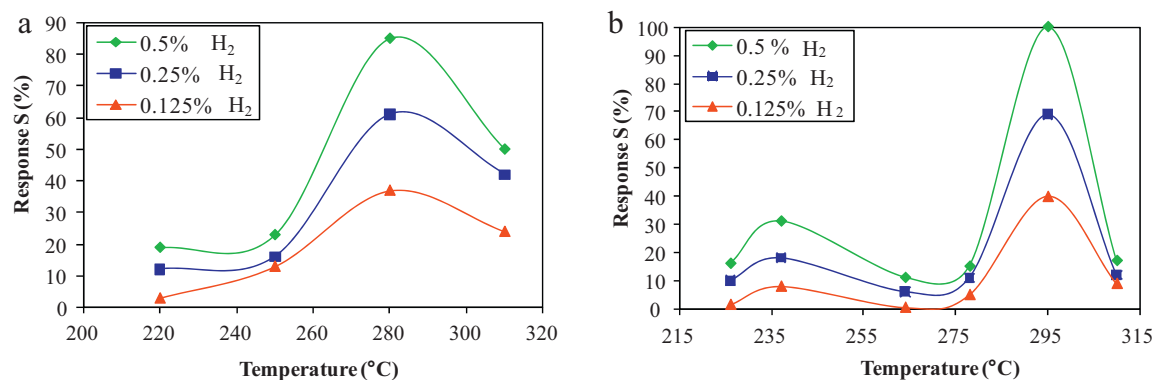
Fig. 6. Response of the sensors at different operating temperatures upon exposure to different concentration of H_2 for a 100 nm thin samples: (a) $P_{0.5}d_5$ and (b) P_2d_8.
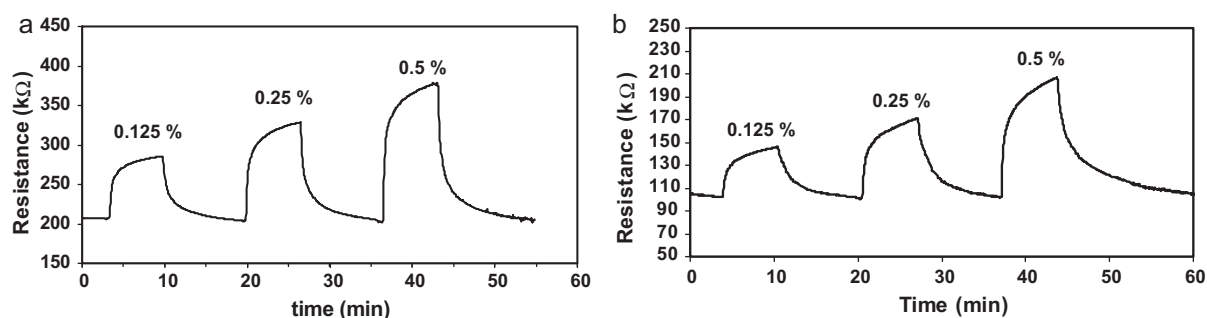

Fig. 7. The change in electrical resistances upon exposure to 0.125, 0.25 and 0.5% H_2 at (a) 280 °C for $P_{0.5}d_5$, (b) 295 °C for P_2d_8.
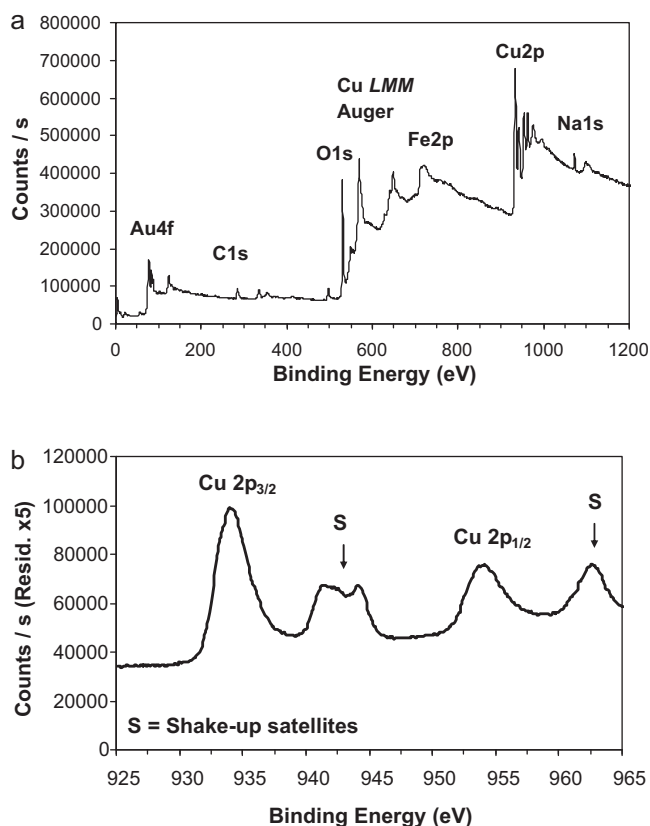

Fig. 8. XPS of CuO–$Cu_xFe_{3-x}O_4$ after H_2 testing; (a) survey scan and (b) high-resolution scan for Cu2p.

Further sensing measurements are found in the "Supporting information": Table of sensor responses, response and recovery times at different temperatures calculated from the dynamic responses for $P_{0.5}d_5$ and P_2d_8 samples.

The XPS spectra of CuO–$Cu_xFe_{3-x}O_4$ after H_2 testing are shown in Fig. 8. The survey scan spectrum Fig. 8a shows photoelectron lines for Cu2p, C1s, O1s, Fe2p, Au4f, Na1s and the Auger lines LMM. The XPS peak for Na observed in the spectrum imply that chemical reactions occur at the interface between the film and the glass substrate and that sodium migrates from the glass substrate into the thin film. The element C in the film is attributed to residual carbon. The XPS peaks for Au come from the gold electrode sputtered at the surface of the thin film for the formation of electrodes (the surface analysis is close to the distance between two gold electrodes). High-resolution scan of Cu2p includes four peaks at 934, 942, 954, and 962 eV (Fig. 8b).

Two peaks at 933.98 and 954.08 eV are due to the spin–orbit doublet of Cu2p and are assigned to the bonding energies of $Cu2p_{3/2}$ and $Cu2p_{1/2}$ in CuO, respectively. The two other peaks on the higher binding energy side of both $Cu2p_{3/2}$ and $Cu2p_{1/2}$ are satellite structures. These satellites can be attributed to shake-up transitions by ligand-to-metal 3d charge transfer [41–43]. This charge transfer can occur for copper present in the Cu^{2+} form ($3d^9$ configuration) but cannot take place if it is present as a metallic or in a Cu^+ state ($3d^{10}$ configuration) because of their completely filled 3d shells.

4. Conclusion

The CuO–$Cu_xFe_{3-x}O_4$ thin films were deposited on glass substrates using the RF-sputtering method followed by a thermal annealing in air at 450 °C. The microcharacterization of samples showed that they were made of well dispersed particles with good homogeneity. Using TEM and AFM characterizations, it was found that before annealing surface of $P_{0.5}d_5$ was rougher than P_2d_8 due

to the presence of metallic copper. However after annealing, the surface of P_2d_8 became relatively rougher compared to $P_{0.5}d_5$. $CuO–Cu_xFe_{3−x}O_4$ nanocomposite thin films showed p-type semiconductor behaviours with increasing electrical resistance upon exposure to hydrogen gas. The best sensing performance was observed for P_2d_8 at an operating temperature of 295 °C with responses of 40, 69, and 100% for H_2 concentrations of 0.125, 0.25, and 0.5%, respectively. The response and recovery times obtained at the lowest concentration (0.125% H_2) were 190 and 400 s, respectively. P_2d_8's better performance can be attributed to its rougher surface in comparison to $P_{0.5}d_5$. Further investigations such as testing the effect of the selectivity and atmosphere humidity are required to optimize sensing parameters.

Acknowledgements

Appendix A. Supplementary data

Supplementary data associated with this article can be found, in the online version, at doi:10.1016/j.snb.2010.10.018.

References

[1] N. Yamazoe, Toward innovations of gas sensor technology (review), Sens. Actuators B: Chem. 108 (2005) 2–14.
[2] S.A. Patil, L.A. Patil, D.R. Patil, G.H. Jain, M.S. Wagh, CuO-modified tin titanate thick film resistors as H_2-gas sensors, Sens. Actuators B: Chem. 123 (2007) 233–239.
[3] C.S. Dandeneau, Y.H. Jeon, C.T. Shelton, T.K. Plant, D.P. Cann, B.J. Gibbons, Thin film chemical sensors based on p-CuO/n-ZnO heterocontacts, Thin Solid Film 517 (15) (2009) 4448–4454.
[4] N.D. Hoa, S.Y. An, N.Q. Dung, N.V. Quy, D. Kim, Synthesis of p-type semiconducting cupric oxide thin films and their application to hydrogen detection, Sens. Actuators B: Chem. 146 (1) (2010) 239–244.
[5] C. Wang, X.Q. Fu, X.Y. Xue, Y.G. Wang, T.H. Wang, Surface accumulation conduction controlled sensing characteristic of p-type CuO nanorods induced by oxygen adsorption, Nanotechnology 18 (2007) 145506–145511.
[6] Y. Nakamura, A. Ando, T. Tsurutani, O. Okada, M. Miyayama, K. Koumoto, H. Yanagida, Gas sensitivity of CuO/ZnO hetero-contact, Chem. Lett. (1986) 413–416.
[7] Y. Nakamura, H. Yoshioka, M. Miyayama, H. Yanagida, Selective CO gas sensing mechanism with CuO/ZnO heterocontact, J. Electrochem. Soc. 137 (1990) 940–943.
[8] L. Liao, Z. Zhang, B. Yan, Z. Zheng, Q.L. Bao, T. Wu, C.M. Li, Z.X. Shen, J.X. Zhang, H. Gong, J.C. Li, T. Yu, Multifunctional CuO nanowire devices: p-type field effect transistors and CO gas sensors, Nanotechnology 20 (8) (2009) 085203.
[9] Y.S. Kim, I.S. Hwang, S.J. Kim, C.Y. Lee, J.H. Lee, CuO nanowire gas sensors for air quality control in automotive cabin, Sens. Actuators B: Chem. 135 (1) (2008) 298–303.
[10] X. Zhou, Q. Cao, H. Huang, P. Yang, Y. Hu, Study on sensing mechanism of CuO-SnO₂ gas sensors, Mater. Sci. Eng. B 99 (1–3) (2003) 44–47.
[11] J. Chen, K. Wang, L. Hartman, W. Zhou, H_2S detection by vertically aligned CuO nanowire array sensors, J. Phys. Chem. 112 (41) (2008) 16017–16021.
[12] F. Marabelli, G.B. Parravicini, F. Salghetti-Drioli, Optical gap of CuO, Phys. Rev. B 52 (1995) 1433–1436.
[13] J. Ghijsen, L.H. Tjeng, J. van Elp, H. Eskes, J. Westerink, G.A. Sawatzky, Electronic structure of Cu_2O and CuO, Phys. Rev. B 38 (1988) 11322–11330.
[14] F.P. Koffyberg, F.A. Benko, A photoelectrochemical determination of the position of the conduction and valence band edges of p-type CuO, J. Appl. Phys. 53 (1982) 1173–1177.
[15] S.T. Jun, G.M. Choi, CO gas-sensing properties of ZnO/CuO contact ceramics, Sens. Actuators B: Chem. 17 (1994) 175–178.
[16] T. Ishihara, K. Kometani, M. Hashida, Y. Takita, Mixed oxide capacitor of BaTiO₃-PbO as a new type CO_2 gas sensor, Chem. Lett. (1990) 1163–1166.
[17] S. Aygün, D. Cann, Hydrogen sensitivity of doped CuO/ZnO heterocontact sensors, Sens. Actuators B: Chem. 106 (2005) 837–842.
[18] L.A. Patil, D.R. Patil, Heterocontact type CuO-modified SnO₂ sensor for the detection of a ppm level H_2S gas at room temperature, Sens. Actuators B: Chem. 120 (2006) 316–323.
[19] G.M. Choi, W.J. Mun, J.H. Yoo, Gas sensor having superior sensitivity and selectivity for carbon monoxide gas and method for manufacturing such gas sensor, Patent number KR20020031439, 2002.
[20] J.H. Yu, G.M. Choi, Current–voltage characteristics and selective CO detection of Zn_2SnO_4 and ZnO/Zn_2SnO_4, SnO_2/Zn_2SnO_4 layered-type sensors, Sens. Actuators B: Chem. 72 (2) (2001) 141–148.
[21] J.J. Vijaya, L.J. Kennedy, G. Sekaran, M. Bayhan, M.A. William, Preparation and VOC gas sensing properties of Sr(II)-added copper aluminate spinel composites, Sens. Actuators B: Chem. 134 (2) (2008) 604–612.
[22] E. Mugnier, A. Barnabé, L. Presmanes, Ph. Tailhades, Thin films preparation by RF-sputtering of copper/iron ceramic targets with Cu/Fe = 1: from nanocomposites to delafossite compounds, Thin Solid Films 516 (2008) 1453–1456.
[23] E. Mugnier, I. Pasquet, A. Barnabé, L. Presmanes, C. Bonningue, Ph. Tailhades, Nanocomposites of metallic copper and spinel ferrite films: growth and self-assembly of copper particles, Thin Solid Films 493 (1–2) (2005) 49–53.
[24] L. Presmanes, S. Capdeville, C. Bonningue, L. Datas, Ph. Tailhades, Magnetic and semi-conducting nano-composite films of spinel ferrite and cubic zinc oxide, Thin Solid Films 515 (17) (2007) 6676–6681.
[25] S. Fernández, A. Martínez-Steele, J.J. Gandía, F.B. Naranjo, Radio frequency sputter deposition of high-quality conductive and transparent ZnO:Al films on polymer substrates for thin film solar cells applications, Thin Solid Films 517 (10) (2009) 3152–3156.
[26] H. Windischmann, Intrinsic stress in sputter-deposited thin films, Crit. Rev. Solid State Mater. Sci. 17 (1992) 547–596.
[27] B. Mauvernay, L. Presmanes, S. Capdeville, V.G. de Resende, E. De Grave, C. Bonningue, Ph. Tailhades, Elaboration and characterization of $Fe_{1−x}O$ thin films sputter deposited from magnetite target, Thin Solid Films 515 (2007) 6532–6536.
[28] S. Capdeville, P. Alphonse, C. Bonningue, L. Presmanes, Ph. Tailhades, Microstructure and electrical properties of sputter-deposited $Zn_{0.87}Fe_{2.13}O_4$ thin layers, J. Appl. Phys. 96 (2004) 6142–6146.
[29] T. Ishihara, K. Kometani, M. Hasida, Y. Takita, Application of mixed oxide capacitor to the selective carbon dioxide sensor, J. Electrochem. Soc. 138 (1991) 173–176.
[30] K. Galatsis, Y.X. Li, W. Wlodarski, K. Kalantar-zadeh, Sol–gel prepared MoO_3–WO_3 thin-films for O_2 gas sensing, Sens. Actuators B: Chem. 77 (1–2) (2001) 478–483.
[31] B. Liao, Q. Wei, K. Wang, Y. Liu, Study on CuO–BaTiO₃ semiconductor CO_2 sensor, Sens. Actuators B: Chem. 80 (3) (2001) 208–214.
[32] K. Galatsis, Y.X. Li, W. Wlodarski, E. Comini, G. Sberveglieri, C. Cantalini, S. Santucci, M. Passacantando, Comparison of single and binary oxide MoO_3, TiO_2 and WO_3 sol–gel gas sensors, Sens. Actuators B: Chem. 83 (1–3) (2002) 276–280.
[33] C. Cantalini, Cr_2O_3, WO_3 single and Cr/W binary oxide prepared by physical methods for gas sensing applications, J. Eur. Ceram. Soc. 24 (6) (2004) 1421–1424.
[34] A. Chapelle, F. Oudrhiri-Hassani, L. Presmanes, A. Barnabé, Ph. Tailhades, CO_2 sensing properties of semiconducting copper oxide and spinel ferrite nanocomposite thin film, Appl. Surf. Sci. 256 (14) (2010) 4715–4719.
[35] K.T. Jacob, K. Fitzner, C.B. Alcock, Activities in the spinel solid solution, phase equilibria and thermodynamic properties of ternary phases in the system Cu–Fe–O, Metall. Trans. B: Process Metall. 8 (1977) 451–460.
[36] F. Oudrhiri-Hassani, L. Presmanes, A. Barnabé, Ph. Tailhades, Microstructure, porosity and roughness of RF sputtered oxide thin films: characterization and modelization, Appl. Surf. Sci. 254 (2008) 5796–5802.
[37] Y.S. Gong, C. Lee, C.K. Yang, Atomic force microscopy and Raman spectroscopy studies on the oxidation of Cu thin films, J. Appl. Phys. 77 (1995) 5422–5425.
[38] J. Chrzanowski, J.C. Irwin, Raman scattering from cupric oxide, Solid State Commun. 70 (1) (1989) 11–14.
[39] J.C. Irwin, J. Chrzanowski, T. Wei, D.J. Lockwood, A. Wold, Raman scattering from single crystals of cupric oxide, Physica C 166 (5–6) (1990) 456–464.
[40] N.D. Hoa, N.V. Quy, H. Jung, D. Kim, H. Kim, S.K. Hong, Synthesis of porous CuO nanowires and its application to hydrogen detection, Sens. Actuators B: Chem. 146 (2010) 266–272.
[41] B. Wallbank, I.G. Main, C.E. Johnson, 2p and 2s shake-up satellites in solid compounds of 3d ions, J. Electron Spectrosc. 5 (1) (1974) 259–266.
[42] K.S. Kim, Charge transfer transition accompanying X-ray photoionization in transition-metal compounds, J. Electron Spectrosc. 3 (3) (1974) 217–226.
[43] J.F. Watts, J. Wolstenholme, An Introduction to surface analysis by XPS and AES, Wiley, 2003 (Chapter 3.2.5).

Biographies

Audrey Chapelle received her MSc in Materials for Energy Storage and Conversion from University Paul Sabatier of Toulouse in 2008. She is currently pursuing her PhD degree on semiconducting copper oxide and spinel ferrite nanocomposite thin films for gas sensing in CIRIMAT laboratory at Paul Sabatier University, Toulouse, France.

Mohd Hanif Yaacob received his Bachelor of Engineering (Electronic Computer Systems) and Master of Science (Communication and Network Engineering) from Salford University, UK (1999) and Universiti Putra Malaysia, Malaysia (2002), respectively. He is currently undertaking his PhD at RMIT University, Melbourne, Australia with his major area of research being the characterization and optical gas sensing properties of nanostructured WO_3 thin films.

Isabelle Pasquet received her PhD degree in Material Science from University Paul Sabatier, Toulouse, in 1995. She has been working in CIRIMAT laboratory since 2000.

Lionel Presmanes received his PhD degree, for his thesis-work on ferrite thin films for magneto-optical storage. Since 1997, he has been working in CIRIMAT laboratory at University Paul Sabatier (Toulouse) and he is also CNRS Researcher since 2001. His research interests are focused on the preparation of sputtered oxide and nanocomposites thin films and the study of their microstructure as well as their electrical, magnetic and optical properties. He developed sputtered ferrite thin films to be integrated as sensitive layers in microbolometers (IR sensors). One potential application of his work is, particularly, semiconductor sensitive layer for gas sensors.

Antoine Barnabé is a professor at the CIRIMAT laboratory, Paul Sabatier University, France. He received his PhD degree in Chemistry of Materials from University de Caen-Basse Normandie (France) in 1999. He held a post-doctoral position in Northwestern University, Evanston (USA), in 2000. His current research interests are mainly focused in functional metal oxide powders, ceramics and thin films prepared by PVD technique.

Philippe Tailhades received his PhD degree in Material Science in 1988 and the Habilitation à Diriger les Recherches in 1994. He is currently the Vice Director of the Centre Interuniversitaire de Recherche et d'Ingénierie des Matériaux (CIRIMAT), Toulouse, France. His research interests include the preparation of original metallic oxides, especially spinel ferrites, in the form of fine powders, thin films, or bulk ceramics and the study of their magnetic, electric, and optical properties. He also works on the preparation of special metallic powders. Dr. Tailhades received the silver medal of CNRS in France in 2000.

Johan Du Plessis received the BSc (Hons) degree in physics and the PhD degree from the University of the Free State, Bloemfontein, South Africa, in 1977 and 1987, respectively. He is currently at the School of Applied Sciences at the Royal Melbourne Institute of Technology (RMIT), Melbourne, Australia, and his research focuses on the characterization of surfaces and thin films using surface analytical techniques.

Kourosh Kalantar-zadeh is an associate professor at the School of Electrical and Computer Engineering, RMIT University, Australia. He received his BSc (1993) and MSc (1997) from Sharif University of Technology, Iran, and Tehran University, Iran, respectively, and completed his PhD at RMIT University, Australia (2001). His research interests include chemical and biochemical sensors, nanotechnology, microsystems, materials science, electronic circuits and microfluidics.